International Journal of Thermophysics, Vol. 18, No. 2, 1997

Heat Capacity Measurement and EXAFS Study of $(U_{0.85}Mg_{0.15})O_{2-x}$ for $x = 0$ and 0.1[1]

Y. Arita,[2] T. Matsui,[2,3] H. Ohno,[4] and K. Kobayashi[5]

Heat capacities and electrical conductivities of $(U_{0.85}Mg_{0.15})O_{2-x}$ ($x = 0$ and 0.1) were measured simultaneously by means of a direct heating pulse calorimeter (DHPC) in the temperature range from 300 to 1500 K. Anomalous increases in the heat capacity curves of $(U_{0.85}Mg_{0.15})O_{2-x}$ ($x = 0$ and 0.1) were observed above about 800 and 1150 K, respectively. The values for the enthalpy of oxygen Frenkel defect formation were calculated from the excess heat capacity and were found to be similar to those for UO_2 doped with rare earth elements. On the other hand, no anomaly was seen in the electrical conductivity curve around the onset temperature of the anomalous increase in the heat capacity. It was, therefore, concluded that the excess heat capacity originates from the predominant contribution of the formation of Frenkel pair-like defects of oxygen. An extended X-ray absorption fine structure (EXAFS) experiment shows a different environment of oxygen around uranium and magnesium, and this should be a cause of the onset temperature difference.

KEY WORDS: EXAFS study; Frenkel defects of oxygen; heat capacity; heat capacity anomaly; Mg-doped UO_2.

1. INTRODUCTION

The heat capacities of $(U_{1-y}M_y)O_2$, where M = Gd [1], La [2], Eu [3], Y [4], Sc [5], simulated fission-products (FP) [4, 6], and Nd [7], have

[1] Paper presented at the Fourth Asian Thermophysical Properties Conference, September 5–8, 1995, Tokyo, Japan.

[2] Department of Quantum Engineering, Graduate School of Engineering, Nagoya University, Nagoya 464-01, Japan.

[3] To whom correspondence should be addressed.

[4] Office of Synchrotron Radiation Facility Project, Japan Atomic Energy Research Institute, Tokai, Ibaraki 319-11, Japan.

[5] Photon Factory, National Laboratory for High Energy Physics, Tsukuba, Ibaraki 305, Japan.

0195-928X/97/0300-0557$12.50/0

been measured over the temperature range from 300 to 1500 K by the present authors. An anomalous increase in the heat capacity curve of each doped UO_2 sample was observed to occur at temperatures ranging from about 550 to 1300 K depending on the dopant and its concentration. This anomalous increase was attributed by the authors [1–7] to the formation of Frenkel pair-like defects of oxygen as in the case of UO_2 [8–10]. However, there have been no data on the heat capacities of UO_2 doped with a divalent cation.

Hence in the present study, the heat capacities and the electrical conductivities of $(U_{0.85}Mg_{0.15})O_{2-x}$ $(x=0$ and $0.1)$ were measured over the temperature range from 300 to 1500 K by means of direct heating pulse calorimetry to investigate further the variation in the onset temperatures of the heat capacity anomaly. The local structural arrangements of oxygen around the cations in pure UO_2- and Mg-doped UO_2 were also discussed, using data from extended X-ray absorption fine structure (EXAFS) experiment.

2. EXPERIMENTAL PROCEDURE

2.1. Sample Preparation and Characterization

The mixture of UO_2 and MgO, both of which were 99.99% pure, was shaped into a cylindrical rod about 6–7 mm in diameter and about 50–70 mm in length, using an evacuated rubber press under a hydrostatic pressure of about 400 MPa. The cylindrical rod, thus prepared, was homogenized and sintered at 1673 K for 7 days in an Ar gas flow so as to obtain the stoichiometric composition of oxygen $(O/M=2.0)$ according to the thermogravimetric studies [11, 12]. The homogenizing and sintering process was repeated several times. After heat capacity measurement, the sample of $(U_{0.85}Mg_{0.15})O_{2.0}$ was reduced to hypostoichiometric composition $(O/M=1.9)$ at 1273 K for 2 days in a hydrogen gas flow, whose composition was evaluated from the weight change of the sample. X-ray diffraction analysis indicated the presence of a single phase for each sample.

2.2. Direct Heating Pulse Calorimeter

The heat capacities and the electrical conductivities were measured simultaneously by means of a direct heating pulse calorimeter (DHPC), described in detail previously [13]. In this calorimeter, an electric current is directly supplied to the sample rod for a short period through a regulated d.c. power supply and the temperature rise of the sample is measured by a thermocouple. To reduce the error in the measured heat

capacity due to heat leak from the sample at high temperatures, the molybdenum shields are heated so as to generate the same temperature rise in the shields as in the sample, i.e., to attain a nearly adiabatic condition. The electrical potential drop, the current, and the temperature rise in the sample rod are measured to obtain the heat capacity and the electrical conductivity of the sample simultaneously. The heat capacity measurement was conducted within an uncertainty of $\pm 2\%$, which was estimated by comparing the heat capacity of undoped UO_2 determined in this study with the previous literature values [1, 4, 14].

2.3. EXAFS Experiment

EXAFS experiments were carried out at the Photon Factory of the National Laboratory for High Energy Physics (KEK, Tsukuba) using the BL-27B line at the uranium L_{III} edge (17.164 keV) for $UO_{2.0}$, $(U_{0.85}Mg_{0.15})O_{2.0}$, and $(U_{0.85}Mg_{0.15})O_{1.9}$, at room temperature. Continuous X-rays from Synchrotron radiation were monochromatized by silicon (111) channel-cut-crystal monochromater. The X-ray beam size is about $1 \times 7\ mm^2$. X-ray intensities before (I_0) and after (I) the sample were measured for 1 s for each of the 500–600 points from a few tens of electron volts before absorption edge to about 1.0 keV higher in energy.

The X-ray absorption is expressed as the following equation:

$$I/I_0 = \exp(-\mu d) \tag{1}$$

where μ is the X-ray absorption coefficient and d is the thickness of the sample. From the above equation, μd is obtained by plotting $\ln(I_0/I)$ versus the energy of incident X-rays. All samples for EXAFS experiment were powdered and mixed with BN powder to reduce the X-ray absorbance. Then the mixed samples were pressed to be $\mu d = 2$–3 at the slightly higher side of absorption edge.

3. RESULTS AND DISCUSSION

3.1. DHPC Measurements

The heat capacities of $(U_{0.85}Mg_{0.15})O_{2-x}$ ($x = 0$ and 0.1), measured in this study are shown in Fig. 1 together with the literature data for undoped UO_2 [1]. Anomalous increases in the heat capacity curve of $(U_{0.85}Mg_{0.15})O_{2.0}$ and $(U_{0.85}Mg_{0.15})O_{1.9}$ are seen above 800 and 1150 K, respectively, similarly to those observed in the cases of UO_2 doped with trivalent cations [1–5, 7].

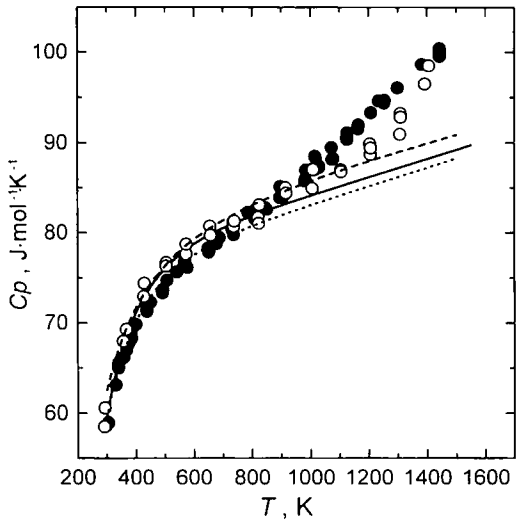

Fig. 1. Temperature dependence of heat capacity. $(U_{0.85}Mg_{0.15})O_{1.9}$: ●, $(U_{0.85}Mg_{0.15})O_{2.0}$ [7]; UO_2 [1]; ---- $(U_{0.85}Mg_{0.15})O_{1.9}$ (fitted baseline); ------ $(U_{0.85}Mg_{0.15})O_{2.0}$ (fitted baseline).

The temperature dependence of the heat capacity of undoped UO_2, which has no phase transition up to 1600 K, has been found to be close to that estimated from Neumann–Kopp's law by Inaba et al. [1]. The excess heat capacity of doped UO_2 was evaluated by subtracting the smoothed baseline determined by applying a least-squares fitting for the data in the temperature range below the onset temperature and extrapolating parallel with the heat capacity curve of undoped UO_2, the fitted line to the range above the onset temperature. Assuming that the excess heat capacity is due to the formation of Frenkel pairs of oxygen, as in the case of UO_2 doped with various cations [1–5, 7], the excess heat capacity (ΔC) can be expressed as [9]

$$\Delta C = \{(\Delta H_f)^2/(\sqrt{2}\,RT^2)\}\exp(\Delta S_f/2R)\exp(-\Delta H_f/2RT) \qquad (2)$$

where ΔH_f and ΔS_f denote the enthalpy and entropy of defect formation, respectively, and R is the gas constant.

The enthalpies of formation for a Frenkel pair in $(U_{0.85}Mg_{0.15})O_{2.0}$ and $(U_{0.85}Mg_{0.15})O_{1.9}$ obtained from Eq. (2) in this study are shown in Fig. 2 together with those of UO_2 [9] and (U, M)O_2 (M = Gd, La, Sc, Eu, Y. Nd, and Mg) reported previously [1–5, 7]. It is seen that the enthalpies for $(U_{0.91}Mg_{0.09})O_{2.0}$ previously reported by us [7] and

$(U_{0.85}Mg_{0.15})O_{2.0}$ are slightly larger than or almost equal to those for UO_2 doped with trivalent cations at the same dopant concentration. Although a dependence of the enthalpy for $(U,Mg)O_{2.0}$ on the dopant concentration seems to be a little different from those observed for UO_2 doped with Gd, La, Eu, and Y, the enthalpies for $y = 0$ obtained by the extrapolation of both curves are not so different from the value for undoped UO_2, showing that the heat capacity anomaly of these doped samples has the same origin as that of undoped UO_2. The difference between the enthalpy of defect formation for $(U_{0.85}Mg_{0.15})O_{2.0}$ and $(U_{0.85}Mg_{0.15})O_{1.9}$ is discussed below in relation to the local structural environment.

Electrical conductivities of $(U_{0.85}Mg_{0.15})O_{2.0}$ and $(U_{0.85}Mg_{0.15})O_{1.9}$ were also measured and the results are shown in Fig. 3 together with those for undoped UO_2 [14] and UO_2 doped with other cations [2, 5], where the onset temperatures of the anomalous increase in the heat capacity are shown by the vertical arrows, respectively. No significant change of slope is seen in the electrical conductivity curve of each sample of $(U_{0.85}Mg_{0.15})O_{2.0}$ and $(U_{0.85}Mg_{0.15})O_{1.9}$ at the temperatures where the heat capacity starts increasing anomalously. Although the increase in the slope is observed for some doped UO_2 samples such as $(U_{0.91}La_{0.09})O_{2.0}$

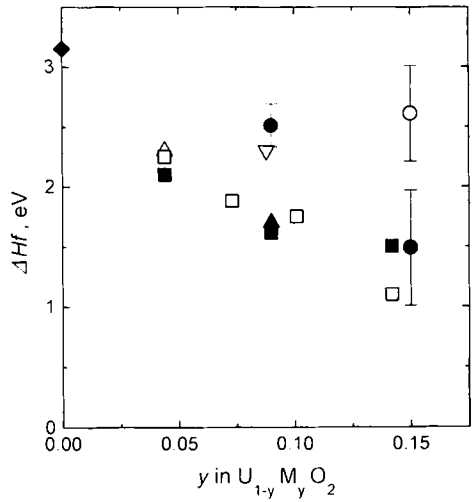

Fig. 2. Enthalpy of defect formation as a function of dopant concentration. O/M = 2.0: ●, M = Mg (this study and Ref. 7); □, M = Gd [1]; ■, M = La [2]; △, M = Eu [3]; ▲, M = Y [4]; ▽, M = Sc [5]. O/M = 1.9: ○, M = Mg (this study); ◆, $UO_{2.0}$ [9].

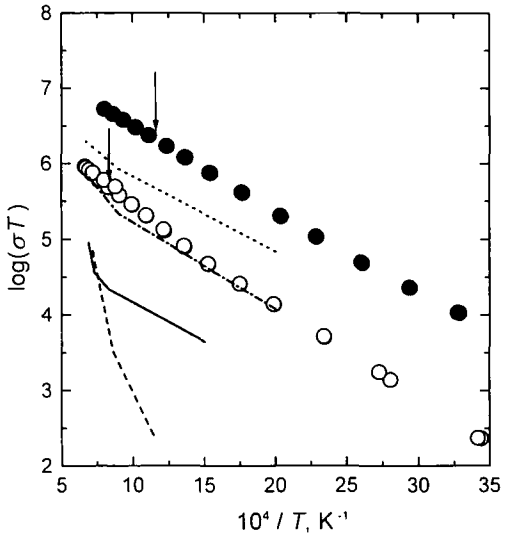

Fig. 3. Variation of $\log(\sigma T)$, where σT is in $S \cdot m^{-1} \cdot K^{-1}$, as a function of inverse temperature. ○, $(U_{0.85}Mg_{0.15})O_{1.9}$; ●, $(U_{0.85}Mg_{0.15})O_{2.0}$ [7]; ····, UO_2 [15]; – – –, $(U_{0.91}La_{0.09})O_{2.0}$ [2]; ------ $(U_{0.91}Sc_{0.09})O_{2.0}$ [5]; ——, $(U_{0.99}Nb_{0.01})O_{2.0}$ [5].

and $(U_{0.99}Nb_{0.01})O_{2.0}$ in Fig. 3, the increase in the slope is thought to be due to the gradual transition from the extrinsic to the intrinsic conduction region from the following facts. (a) The temperature at which the slope of the conductivity changes is almost independent of the dopant and its concentration and is close to that of undoped UO_2. (b) The temperature at which the slope changes does not always coincide with the onset temperature of the heat capacity anomaly. (c) The increase in the slope in the conductivity curve is also observed in $(U_{0.99}Nb_{0.01})O_{2.0}$, which showed no heat capacity anomaly. It is, therefore, not likely that the excess heat capacity of $(U_{0.85}Mg_{0.15})O_{2.0}$ and $(U_{0.85}Mg_{0.15})O_{1.9}$ is due to the formation of electron-hole pairs.

3.2. EXAFS Measurements

Absorption spectra near the U-L_{III} edge are shown in Fig. 4. The EXAFS function χ is typically plotted in terms of the photoelectron wave vector k, where k is related to kinetic energy of the photoelectron (E) by

$$k = 2\pi/h[2m(E - E_0)]^2 \tag{3}$$

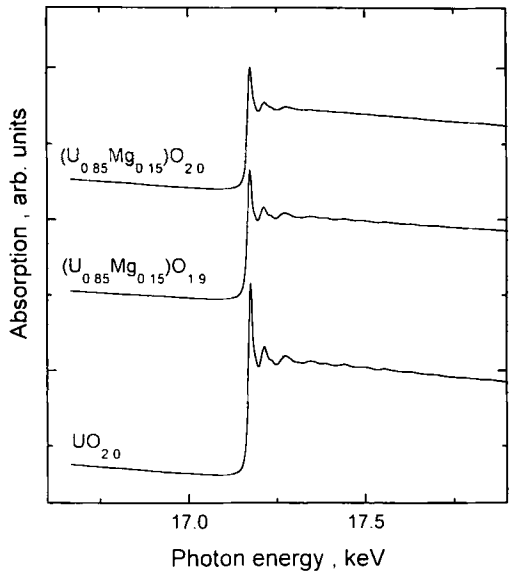

Fig. 4. X-ray absorption spectrum in the vicinity of the U-L_{III} edge.

E_0 is the threshold energy of the photoelectron at $k=0$, h is Planck's constant, and m is the mass of the electron. In obtaining the EXAFS function $\chi(k)$, the background level was subtracted from the observed absorption coefficient by using a Victreen fit and the absorption coefficient for the isolated atom was obtained by the cubic spline technique. Using a single scattering approximation, the EXAFS for an L_{III} edge is [16]:

$$\chi(k)=\sum_j \frac{N_j \cdot \gamma_j \cdot F_j(k)}{kr_j^2} \exp(-2k^2\sigma_j^2) \cdot \exp(-2r_j/\lambda(k)) \cdot \sin[2kR_j+\phi_j(k)] \tag{4}$$

where N_j is the average number of atoms of a particular element in a shell j which is at an average radius R_j from the absorbing atom. σ_j is a Debye–Waller like factor which represents the relative root-mean-square displacement from R_j due to thermal (vibrational) and static disorder. λ_j is the mean free path of the electron, and γ an amplitude reduction term. The $F_j(k)$ and $\phi_j(k)$ are the backscattering and phase shift functions, respectively. Figure 5 shows plots of χk^n vs $k(n=3)$. The factor k^n, used to weight the data according to the value of k, counteracts the rapid damping of χ with increasing k. The next form is the Fourier transform of k^3, which gives a "radial structure function" (R.S.F.). In this representation, each shell of

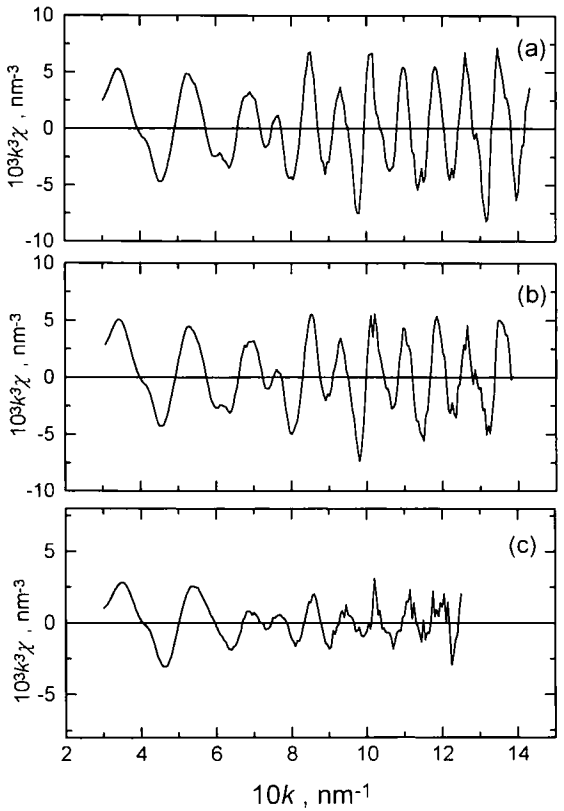

Fig. 5. EXAFS spectra of the U-L_{III} edge. (a) UO_2; (b) $(U_{0.85}Mg_{0.15})O_{1.9}$; (c) $(U_{0.85}Mg_{0.15})O_{2.0}$.

atoms appears as a peak whose maximum is slightly shifted due to the k dependence of ϕ. The Fourier transformed EXAFS spectra of the $UO_{2.0}$, $(U_{0.85}Mg_{0.15})O_{2.0}$, and $(U_{0.85}Mg_{0.15})O_{1.9}$, taken at the uranium absorption edge, are shown in Fig. 6. The two main peaks in the spectra of $UO_{2.0}$ and $(U_{0.85}Mg_{0.15})O_{1.9}$ may be attributed, in order of increasing distance, to the couples of uranium–oxygen and uranium–uranium, and the structure is essentially of a fluorite type. However, in the case of $(U_{0.85}Mg_{0.15})O_{2.0}$, the first peak split into two broad peaks, which suggests that there are at least two different oxygen shells around the uranium atom.

The local structural environments of Y^{3+} and Zr^{4+} ions in 18 wt% Y_2O_3 doped ZrO_2 were previously studied by using EXAFS spectroscopy over the temperature range from 153 to 1043 K [17]. The oxygen arrangements around Y^{3+} and Zr^{4+} were found to be different from each

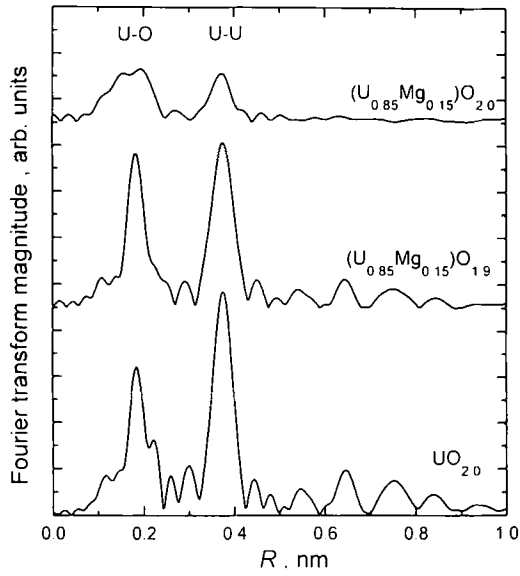

Fig. 6. Radial structural functions (RSFs) of the U-L_{III} EXAFS.

other,i.e., more oxygen vacancies were sited adjacent to Zr^{4+} and were more disordered than those near Y^{3+} at low temperatures. The structural environment of Zr^{4+} in cubic ZrO_2 resembled that of the 7-coordinated Zr^{4+} in monoclinic ZrO_2. Increasing the temperature of the sample resulted in the local structural environments of two cations becoming more alike, suggesting that increased oxygen mobility leads to an increasing random distribution of oxygen defects.

The treatment of EXAFS data frequently involves the inverse Fourier transform of R.S.F. over a limited range of R. This procedure isolates the contribution to EXAFS arising from shells of atoms within that range of R. The parameters of this equation can then be obtained by a least-squares fitting procedure, provided that the phase $[\phi(k)]$ and amplitude $[f(k)]$ are known. From a practical viewpoint $[\phi(k)]$ and $[f(k)]$ have been derived from stoichiometric UO_2. Hence, the results represent the structural deviation from "standard" UO_2. An estimate of an absolute σ, although not essential, has been made to allow comparison with *ab initio* values for other atoms.

The separate contributions of the U–O and U–U shells were filtered and inverse Fourier transformation was then fitted to the EXAFS equation, using least-squares minimization routines with the reference parameters derived from EXAFS spectra of pure UO_2 (Fig. 7).

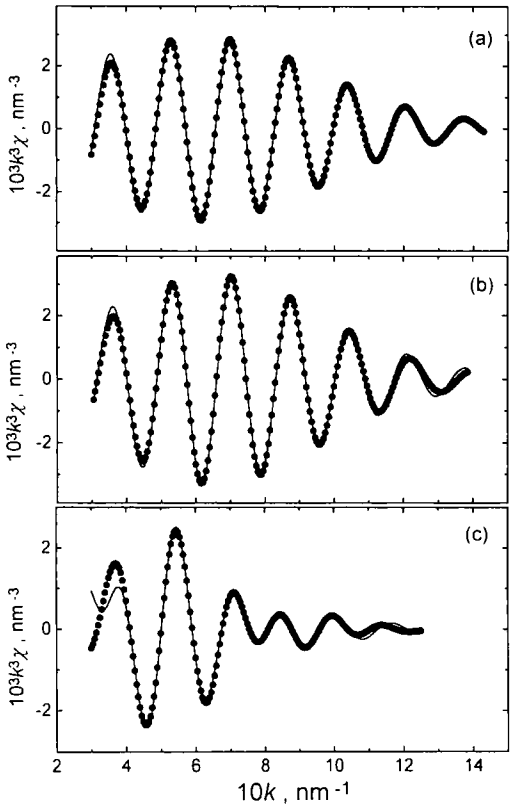

Fig. 7. Filtered, experimental EXAFS spectrum (dots) of the first RSF peak (U–O shell) and nonlinear least-squares fit (solid line). (a) UO_2; (b) $(U_{0.85}Mg_{0.15})O_{1.9}$; (c) $(U_{0.85}Mg_{0.15})O_{2.0}$.

As seen in Fig. 8, all r(U–U) values of UO_2, $(U_{0.85}Mg_{0.15})O_{2.0}$, and $(U_{0.85}Mg_{0.15})O_{1.9}$ from EXAFS are almost the same as those calculated theoretically from lattice constants. On the other hand, r(U–O) values in $(U_{0.85}Mg_{0.15})O_{2.0}$ from EXAFS are not the same single value from lattice constant but are split into two different distances. In fluorite structure, cation has eight oxygens as the nearest neighbor atom. Table I gives the fitted value of the coordination number for the nearest-neighbor oxygen shell of the uranium atom. In the case of UO_2, uranium has eighthold coordination of oxygen, but in both $(U_{0.85}Mg_{0.15})O_{1.9}$ and $(U_{0.85}Mg_{0.15})O_{2.0}$, the coordination numbers are larger than eight. It is suggesting that an oxygen atom is more favorable around an uranium atom than a magnesium atom. Furthermore, in the case of $(U_{0.85}Mg_{0.15})O_{2.0}$, oxygen environment around

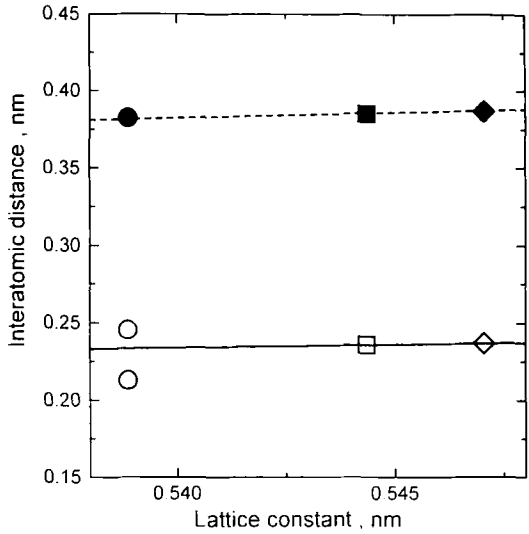

Fig. 8. Variation of interatomic distances. (○, ◆) UO_2; (□, ■) $(U_{0.85}Mg_{0.15})O_{1.9}$; (○, ●) $(U_{0.85}Mg_{0.15})O_{2.0}$; (open, U-O; filled, U-U); —, U-O (from lattice constant); – –, U-U (from lattice constant).

the cations, including oxygen vacancies around magnesium atom, is thought to be disordered, i.e., nonuniform. Therefore, oxygen Frenkel defects are easily formed with increasing temperature such as to make the distribution of oxygen defects around magnesium and uranium uniform (disordered), resulting in the heat capacity anomaly, consisting with the smaller enthalpy of formation of oxygen Frenkel defect for $(U_{0.85}Mg_{0.15})O_{2.0}$ compared to $(U_{0.85}Mg_{0.15})O_{1.9}$.

Table I. Interatomic Distance (R), Coordination Number of Oxygen Around Uranium (N) and Temperature of Heat Capacity Increase Anomaly

Sample	r(U-O) (nm)	N	Tr (K)
$UO_{2.0}$	0.237	8.0	1600
$(U_{0.85}Mg_{0.15})O_{1.9}$	0.236	8.5	1150
$(U_{0.85}Mg_{0.15})O_{2.0}$	0.213	4.6	800
	0.246	5.9	

4. CONCLUSIONS

The conclusions obtained in this study are summarized as follows. (a) For each sample of $(U_{0.85}Mg_{0.15})O_{2.0}$ and $(U_{0.85}Mg_{0.15})O_{1.9}$, an anomalous increase in the heat capacity was observed above 800 and 1150 K respectively, as was previously observed in the cases of $(U_{1-y}M_y)O_2$ (M = Gd, La, Y, Eu, and Sc) by the present authors. (b) The enthalpy of formation for oxygen Frenkel defects in $(U_{0.85}Mg_{0.15})O_{1.9}$ was a little larger than those in $(U_{0.85}Mg_{0.15})O_{2.0}$ and UO_2 doped with other cations. However, the value obtained by extrapolating the enthalpy values of $(U,Mg)O_{2.0}$ to zero dopant concentration was in agreement with that of undoped UO_2, indicating the similar mechanism for heat capacity anomaly. The excess heat capacity is thought to be due to the predominant formation of Frenkel defects of oxygen. (c) The onset temperatures of the heat capacity anomaly for UO_2 doped with Mg were thought to be dependent on the oxygen environment around the uranium atom, i.e., the uranium–oxygen interatomic distance and oxygen coordination number.

REFERENCES

1. H. Inaba, K. Naito, and M. Oguma, *J. Nucl. Mater.* **149**:341 (1987).
2. T. Matsui, Y. Arita, and K. Naito, *J. Radioanal. Nucl. Chem.* **143**:149 (1991).
3. T. Matsui, T. Kawase, and K. Naito, *J. Nucl. Mater.* **186**:254 (1992).
4. T. Matsui, Y. Arita, and K. Naito, *J. Nucl. Mater.* **188**:205 (1992).
5. T. Matsui, Y. Arita, and K. Naito, *Solid State Ionics* **49**:195 (1991).
6. Y. Arita, S. Hamada, and T. Matsui, *Thermochim. Acta* **247**:225 (1994).
7. Y. Arita and T. Matsui, *Thermochim. Acta* **267**:389 (1995).
8. J. F. Kerrisk and D. G. Clifton, *Nucl. Technol.* **16**:531 (1972).
9. R. Szwarc, *J. Phys. Chem. Solids* **30**:705 (1969).
10. P. Browning, *J. Nucl. Mater.* **98**:345 (1981).
11. T. Fujino and K. Naito, *J. Inorg. Nucl. Chem.* **32**: 627 (1970).
12. T. Fujino, J. Tateno, and H. Tagawa, *J. Solid State Chem.* **24**:11 (1978).
13. K. Naito, H. Inaba, M. Ishida, and K. Seta, *J. Phys. E* **12**:712 (1979).
14. F. Gronvold, N. J. Kveseth, A. Sveen, and J. Tichy, *J. Chem. Thermodyn.* **2**:665 (1970).
15. T. Matsui and K. Naito, *J. Nucl. Mater.* **138**:19 (1986).
16. D. J. Jones, J. Roziere, G. C. Allen, and P. A. Tempest, *J. Chem. Phys.* **84**:6075 (1986).
17. C. R. A. Catlow, A. V. Chadwick, G. N. Greaves, and L. M. Moroney, *J. Am. Ceram. Soc.* **69**:272 (1986).